Arabian Journal of Chemistry (2023) **16**, 104589

King Saud University

Arabian Journal of Chemistry

www.ksu.edu.sa
www.sciencedirect.com

ORIGINAL ARTICLE

Numerical treatment of Casson nanofluid Bioconvectional flow with heat transfer due to stretching cylinder/plate: Variable physical properties

Umar Farooq [a,*], Hassan Waqas [b], Sharifah E.Alhazmi [c], Abdullah Alhushaybari [d], Muhammad Imran [a], R. Sadat [e], Taseer Muhammad [f], Mohamed R. Ali [g,*]

[a] *Department of Mathematics, Government College University Faisalabad, 38000, Pakistan*
[b] *School of Energy and Power Engineering, Jiangsu University, Zhenjiang 212013, China*
[c] *Mathematics Department, Al-Qunfudah University College, Umm Al-Qura University, Mecca, Saudi Arabia*
[d] *Department of Mathematics, College of Science, Taif University, P.O. Box 11099, Taif 21944, Saudi Arabia*
[e] *Department of Mathematics, Faculty of Engineering, Zagazig University, Zagazig, Egypt*
[f] *Department of Mathematics, College of Sciences, King Khalid University, Abha 61413, Saudi Arabia*
[g] *Faculty of Engineering and Technology, Future University in Egypt New Cairo, 11835, Egypt*

Received 14 November 2022; accepted 12 January 2023
Available online 18 January 2023

KEYWORDS

Casson nanofluid;
Bioconvection;
Motile microorganisms;
Exponential heat source-sink;
Shooting approach (bvp4c);
Cylinder/Plate

Abstract *Purpose:* The purpose of the current framework is to scrutinize the two-dimensional flow and heat transfer of Casson nanofluid over cylinder/plate along with impacts of thermophoresis and Brownian motion effects. Also, the effects of exponential thermal sink/source, bioconvection, and motile microorganisms are taken.

Methodology/Approach: The resulting non-linear equations (PDEs) are reformed into nonlinear ODEs by using appropriate similarity variables. The resultant non-linear (ODEs) were numerically evaluated by the use of the Bvp4c package in the mathematical solver MATLAB.

Findings: The numerical and graphical illustration regarding outcomes represents the performance of flow-involved physical parameters on velocity, temperature, concentration, and microorganism profiles. Additionally, the skin friction coefficient, local Nusselt number, local Sherwood number, and local microorganism density number are computed numerically for the current presented system. We noted that the velocity profile diminishes for the rising estimations of magnetic

* Corresponding authors.
E-mail addresses: mohamed.reda@fue.edu.eg (U. Farooq), mohamed.reda@fue.edu.eg (M.R. Ali).
Peer review under responsibility of King Saud University.

Production and hosting by Elsevier

https://doi.org/10.1016/j.arabjc.2023.104589

Nomenclature

u, v	Velocity of components (ms^{-1})	Pr	Prandtl parameter
ρ	Density of fluid (kgm^{-3})	Q_E	Exponential heat-sink parameter
x, r	Space coordinates (m)	Ec	Eckert parameter
$(c_p)_f$	Heat capacity of the fluid $(Jkg^{-1}K^{-1})$	W_c	Speed of cell swimming (ms^{-1})
α	Curvature parameter	Lb	Bioconvection Lewis parameter
ζ	Dimensionless coordinator	T	Temperature
θ	Dimensionless temperature	C	Concentration
ϕ	Dimensionless concentration	N	Microorganisms
χ	Dimensionless microorganisms	Rd	Thermal radiation parameter
β	Casson fluid parameter	Le	Lewis parameter
δ	Microorganisms difference number	θ_w	Temperature ratio parameter
σ	Electrical conductivity (Sm^{-1})	Q_P	Heat-source parameter
δ	Temperature difference parameter	Pe	Peclet parameter
v	Kinematic viscosity $(kgms^{-1})$	b	Chemotaxis constant
λ	Mixed convection parameter	C_f	Skin friction coefficient
λ_1	Thermal-Biot number	Nu_x	Nusselt number
λ_2	Solutal-Biot number	Sh_x	Sherwood number
λ_3	Microorganisms-Biot number	Nn_x	Microorganisms density number
T_w	Wall temperature (K)	τ_w	Shear stress tensor (Nm^{-2})
C_w	Wall concentration $(mol.kg^{-1})$	q_w	Wall heat flux (K)
N_w	Wall motile microorganisms $(mol.kg^{-1})$	q_m	Mass heat flux
Nc	Bioconvection Rayleigh number	q_n	Motile microorganism's heat flux
Nr	Buoyancy-ratio parameter	T_∞	Ambient temperature (K)
D_T	Thermophoresis diffusion coefficient (m^2s^{-1})	C_∞	Ambient concentration $(mol.kg^{-1})$
D_m	Microorganisms diffusion coefficient (m^2s^{-1})	N_∞	Ambient microorganisms $(mol.kg^{-1})$
D_B	Brownian diffusivity (m^2s^{-1})	n	Fitted-rate constant
Nt	Thermophoresis number	Nb	Brownian motion number

and mixed convection parameters. The Prandtl number corresponds with the declining performance of the temperature profile observed. The enhancement in the values of the Solutal Biot number and Brownian motion parameter increased in the concentration profile.

Originality: In specific, this framework focuses on the rising heat transfer of Casson nanofluid with bioconvection by using a shooting mathematical model. The novel approach of the presented study is the use of motile microorganisms with exponential thermal sink/source in a Casson nanofluid through a cylinder/plate. A presented study performed first time in the author's opinion. Understanding the flow characteristics and behaviors of these nanofluids is crucial for the scientific community in the developing subject of nanofluids.

1. Introduction

Nanofluid innovation has several technological and industrial uses, including industrial, aeronautics, veterinary, miscomputing, pharmaceutical, and several others. Nanotechnology is mostly applied in the medicinal, nanotube, chemotherapy, and glass industries. Choi (Choi et al., 1995) established a noble and creative technology that needs the mixing of nanoparticles and the base fluid for improved heat transport liquids with much higher temporal conductivities in terms of energy savings and environmental cleanup. Because of their greatly enhanced thermophysical characteristics, nanofluids serve as ideal coolants in several applications. Choi's groundbreaking research was inspired by the conclusion that base fluids with low thermal conductivities are efficient for today's heat transfer requirements. Buongiorno (Buongiorno, 2006) looked at the remarkable sliding properties of Brownian motion and thermophoresis development around the nanofluid. The consequences of heat radiation and Magnetohydrodynamics nanofluid flow over permeable media were studied by Krishna and Chamkha (Krishna and Chamkha, 2020). Krishna (Krishna, 2021) looked influences of Hall and ion slip over a Jeffrey nanofluid moving on a surface that transfers heat. Krishna et al. (Krishna et al., 2020) investigated the Hall and ion slip processes in MHD flow nanofluid through a heat and mass transfer plate. Krishna and Chamkha (Krishna and Chamkha, 2019) investigated the influence of nano-fluid ions and Hall slip over a porosity media. Krishna et al. (Krishna et al., 2019) described the Joule heating impact of MHD nanofluid with temporal heatings into an implanted in a porous media. Krishna (Krishna, 2020) used thermal radiation to study the impact of Hall and ion slip on nanofluid movement. Krishna and Chamkha (Krishna and Chamkha, 2021) explored how slip disrupts the MHD stream of Jeffrey nano-fluid throughout a plate. Veera et al. (Veera Krishna et al., 2018) studied the effect of

MHD nanofluid flow over two perpendicular plates on heat and mass transport.

Non-Newtonian fluids, like Casson fluids, are best characterized as shear-thinning fluids, in flow velocity at zero it has infinite viscosity, a yielding tension beyond which no fluid flows, and zero viscosity at zero shear rates. Tomato sauce, honey, and blood are among well-known liquids with Casson fluid properties. Casson nano-fluid is the fundamental liquid of Casson nanomaterials. Various publications published on the Casson nano-fluid stream study. The process of Bio-convection in a Casson nano-fluid has applications in industrialization, biotechnology, and food science, including fermentation. Ullah et al. (Ullah et al., 2019) examined heat generation/absorption and magnetized Casson nano-fluid stream through a nonlinear permeable stretchable cylindrical media having porosity. Kumar et al. (Kumar et al., 2019) reported the significance of the Williamson-Casson liquid MHD stream via an extended cylinder. Alizadeh et al. (Alizadeh et al., 2021) investigated a Casson liquid computational formula including heat transfer and stagnation point stream throughout a cylinder. Murthy et al. (Murthy et al., 2019) investigated the impacts of the Casson fluid stream across an expanding cylinder with heat radiation. Qadan et al. (Qadan et al., 2019) discussed an MHD stream subject to a micropolar-Casson nanofluid over a cylinder using solar heat. Hiremath et al. (Hiremath et al., 2019) reported the impact of heat conductivity in Casson liquid flow over it with a cylinder. Reddy et al. (Reddy et al., 2019) scrutinized the effects of Casson nano-fluid flow traveling via circular channels with heat radiation and a minimal amount of energy. Ali et al. (Ali et al., 2019) considered the effects of the Casson fluid heat transfer stream across an oscillating cylinder with Heat and mass transfer. Anantha et al. (Anantha Kumar et al., 2020) investigated the effect of heat energy on Casson fluid in a boundary layer flow with a cervical medium. Venkata et al. (Venkata Ramudu et al., 2020) viewed the consequence of suction/injection over Casson nanofluid flow across a horizontal stretchy sheet using MHD. Hussain et al. (Hussain et al., 2020) investigated MHD Casson nano liquid flow with slip conditions across an expanding/shrinking sheet. Ali et al. (Ali et al., 2020) investigated the interaction of Casson nano liquid with enthalpy change through a channel. Lund et al. (Lund et al., 2020) investigated the interactions between MHD Casson nanofluid stagnation point flow and heat radiation and entropy. Salahuddin et al. (Salahuddin et al., 2020) established the model to examine the physical properties of Casson nano-fluid flow by considering activation energy. Gireesha and Sindhu (Gireesha and Sindhu, 2020) investigated the role of boundary layer flow in annular microchannels with heat production and absorption. Tulu and Ibrahim (Tulu and Ibrahim, 2020) used the Cattaneo-Christov heat model to explore Casson nanofluid through the stretched cylinder. Thumma et al. (Thumma et al., 2020) showed the MHD Casson nanofluid stream with heat radiation and reaction temperature. Shankar et al. (Shankar et al., 2020) inspected the aftermath of Cattaneo-Christov heat transmission through stretchable media MHD Casson fluid stream. Sohail et al. (Sohail et al., 2020) checked out the effects of entropy and thermal transport in Casson nano-fluid stream across a unidirectional stretched sheet using magnetohydrodynamics. Shatanawi et al. (Shatnawi et al., 2022) investigated Casson nanofluid correlations with heat radiation and stagnation point flow via a Sheet. Shatanawi et al. (Shatnawi et al., 2022) corroborated the impacts of hybrid Casson nano-fluid with magnetism and heat transport via a plane surface. Abbas et al. (Abbas et al., 2022) constructed a mathematical system of nanofluid flow across a plate. The theoretical flow of ferrofluid on a circular cylinder with convective heat was examined by Abbas and Shatanawi (Abbas and Shatanawi, 2022). The heat transmission in Casson nano-fluid through a Riga sheet was examined by Abbas and Shatanawi (Abbas and Shatanawi, 2022). Mukhopadhyay et al. (Mukhopadhyay et al., 2005) probed the boundary layer stream in the presence of heat radiation passing through a sheet. Mukhopadhyay et al. (Mukhopadhyay et al., 2013) investigated the Casson fluid MHD flow via a sheet. The Casson nanofluid solution with MHD flow and heat radiation over a sheet was estimated by Bhattacharyya et al. (Bhattacharyya et al., 2016). Haldar et al. (Haldar et al., 2017) explored heat radiation over a sheet using dual nanofluid formulations.

Self-propelled amoeboid microbes that drift in a liquid cause bioconvection to happen. When the amount of nanomaterials available is small sufficient that they have no impact upon this base shear flow, bioconvection in nanofluids can be examined. Because motile bacteria are normally stronger than water, they are more likely to move upward and contribute to the unstable top large density stratified. Temperature bioconvection is significant in planetary geology processes, such as hot springs caused by motile microorganisms manifested as thermopiles, which are thermal living microorganisms. Microorganism uses are engaged in oil bearings to nearby absorptive differences, which integrate microorganisms with the benefits of nanofluids. Heat transport is being studied to expand it even more. Many credible professionals lately researched bioconvection in nanofluids investigation. Kuznetsov (Kuznetsov, 2012) proposed first the idea of bioconvection in Microsystems. The investigation of the Bioconvectional stream of Oldroyd-B hybrid nano-fluid subject to reaction temperature, thermal radiation, and motile microorganisms was structured by Waqas et al. (Waqas et al., 2021). Zhang et al. (Zhang et al., 2020) purported effects of motile microbes and bioconvection in nano liquid over a Riga plate with Darcy-Forchheimer flow. Bhatti et al. (Bhatti et al., 2022) explored the impact of nanofluid traveling via tapering arteries on natural convection flow using motile bacteria. Bhatti et al. (Bhatti et al., 2020) audited motility and bioconvection of microorganisms in nano-fluid over the permeable plate. The effects of swimming gyrotactic microorganisms and bioconvection in nanofluids across an extended surface were studied by Shahid et al. (Shahid et al., 2020). Muhammad et al. (Muhammad et al., 2021) demonstrated the relevance of Carreau nanofluid bioconvection and heat transport with repercussions of thermal radiation throughout the wedge surface. Khan et al. (Khan et al., 2020) examined the bio-convectional stream of nano-liquid through two plates. The consequences of heat radiation and activation energy on nanofluid with natural convection flow throughout the Riga plate were taken into account by Bhatti et al. (Bhatti and Michaelides, 2021). Shehzad et al. (Shehzad et al., 2020) used the Cattaneo-Christov theory and a disk-shaped geometry to investigate the relevance of bioconvection and motile microorganisms in a nanofluid. Ayodeji et al. (Ayodeji et al., 2020) examined thermophoresis and Brownian motion in an MHD Bioconvectional stream of nano-fluid through a stretched wall. Ali et al. (Ali et al., 2023) looked into the interactions of heat radiation and motile microorganisms in nanofluids flowing through a cylinder. Sarkar and Das (Sarkar and Das, 2022) studied the MHD flow of a nanofluid around a cylindrical surface using bioconvection and heat absorption. In the presence of a Cross nanofluid running through such a cylinder, Ali et al. (Ali et al., 2022) hypothesized bioconvection and motile microorganisms. Sarkar et al. (Sarkar et al., 2022) studied Bioconvection in nanofluid through Riga plate in presence of motile microorganisms and heat transfer.

A comprehensive review of previous research reveals that no investigation has been explored for evaluating the Casson nanofluid with bioconvection induced by swimming microorganisms across a cylinder/plate utilizing non-linear thermal radiation. Our study is unique in that it investigates the influence of Casson nanofluid convectional flow on motile gyrotactic microorganisms, and also thermal sink/-source which is assumed as exponential. The investigation of movement is based on controlled PDEs in the form of ODEs, which are then computationally addressed by using the shooting approach using bvp4c Matlab software. This technique is employed in engineering problems to determine how different independent variable choices impact the intended outcome. The current technique has the potential to tackle several biological, pharmacological, and environmental challenges. Among the most significant implications for medical and biological sciences is the carrying facts variable which is the emergent

impact over nano-bioconvective comprising dissemination of gyrotactic microorganisms that may exploit as correctly initiate medication conveyance.

2. Mathematical description

We analyze the two-dimensional flow of Casson nanofluid via a cylinder/plate with nonlinear thermal radiation, Brownian motion, thermophoresis effect, and exponential heat source/sink. The geometry of the present issue is depicted via cylindrical coordinates in this way cylinder is considered horizontal in the vertical direction (x-axis) and orthogonal to it in the radial direction (y-axis), as illustrated in Fig. 1.

The assumptions of the current flow model can be described as follows:

- Two-dimensional steady time-dependent flow is mathematically formulated.
- The Casson fluid flow over a cylinder/plate is studied here.
- The importance of Non-linear thermal radiation and exponential heat source/sink are summarized.
- The effect of bioconvection with swimming motile microorganisms is developed.
- The Bvp4c (shooting approach) is used.

The governing equations are (Azam et al. (Azam et al., 2022), Reddy et al. (Reddy et al., 2018), Cao et al. (Cao et al., 2022), and Song et al. (Song et al., 2021):

$$\partial_x(ru)+\partial_r(rv)=0\}, \tag{1}$$

$$\left.\begin{aligned} u\partial_x u+v\partial_r u &= \upsilon\left(1+\tfrac{1}{\beta}\right)\left(\partial_{rr}u+\tfrac{1}{r}\partial_r u\right)-\tfrac{\sigma B^2}{\rho}u \\ &+\tfrac{1}{\rho_f}\left[\rho_f\beta^{**}g*(T-T_\infty)(1-C_f)\right. \\ &\left.-g^*(C-C_\infty)(\rho_p-\rho_f)-g^*\gamma(\rho_m-\rho_f)(N-N_\infty)\right] \end{aligned}\right\}, \tag{2}$$

$$\left.\begin{aligned} u\partial_x T+v\partial_r T &= \tfrac{1}{\rho c_p}\partial_r[K(T)\partial_r T] \\ &+\alpha\left(\partial_{rr}T+\tfrac{1}{r}\partial_r T\right)+\tfrac{\mu_B}{\rho c_p}\left(1+\tfrac{1}{\beta}\right)(\partial_r u)^2+\tfrac{\sigma B_0^2 u^2}{\rho c_p} \\ &+\tfrac{1}{\rho cp}\partial_z(q_r)+\tau\left(D_B\partial_r C\partial_r T+\partial_z C\partial_z T+\tfrac{D_T}{T_\infty}\left((\partial_r T)^2+(\partial_z T)^2\right)\right) \\ &+\tfrac{Q_T^*}{\rho_f c_{pf}}(T-T_\infty) \\ &+\tfrac{Q_E^*}{\rho_f c_{pf}}(T_f-T_\infty)\exp\left(-\sqrt{\tfrac{u_0}{\upsilon l}}\left(\tfrac{r^2-R^2}{2R}\right)n\right) \end{aligned}\right\}, \tag{3}$$

$$u\partial_x C+v\partial_r C=\frac{1}{\rho c_p}\partial_r[K(C)\partial_r C]+D_B\frac{1}{r}\partial_r[r\partial_r C]+\frac{D_T}{T_\infty}\frac{1}{r}\partial_r[(r\partial_r T)]\Big\}, \tag{4}$$

$$u\partial_x N+v\partial_r N+[\partial_r(N\partial_r C)]\frac{bW_c}{(C_w-C_\infty)}=D_m\partial_{rr}N\Big\} \tag{5}$$

With suitable boundary conditions:

$$\left.\begin{aligned} &u(x,r)=u_w(x)=\tfrac{u_0 x}{l},\quad v(x,r)=0,\ -k\partial_r T=h_f(T_w-T), \\ &-D_B\partial_r C=h_g(C_w-C), \qquad -D_m\partial_r N=h_m(N_w-N) \\ &\qquad\qquad at \qquad r=R, \\ &u\to 0,\quad N\to N_\infty,\quad C\to C_\infty,\quad T\to T_\infty,\quad at\ \ r\to\infty \end{aligned}\right\} \tag{6}$$

Mathematically, radiative heat fluxq_r, variable conductivity$K(T)$, and variable diffusivity $K(C)$ are addressed (Waqas et al. (Waqas et al., 2020).

$$\left.\begin{aligned} q_r=-\tfrac{4\sigma^*}{3k^*}\tfrac{\partial T^4}{\partial r}=\tfrac{16\sigma^*}{3k^*}T_\infty^3\tfrac{\partial T}{\partial r},\ K(T)=k_\infty\left[\in_1\left(\tfrac{T-T_\infty}{\Delta T}\right)+1\right], \\ K(C)=D_\infty\left[\in_2\left(\tfrac{C-C_\infty}{\Delta C}\right)+1\right] \end{aligned}\right\} \tag{7}$$

The appropriate similarity transformations are (Tamoor et al. (Tamoor et al., 2017).

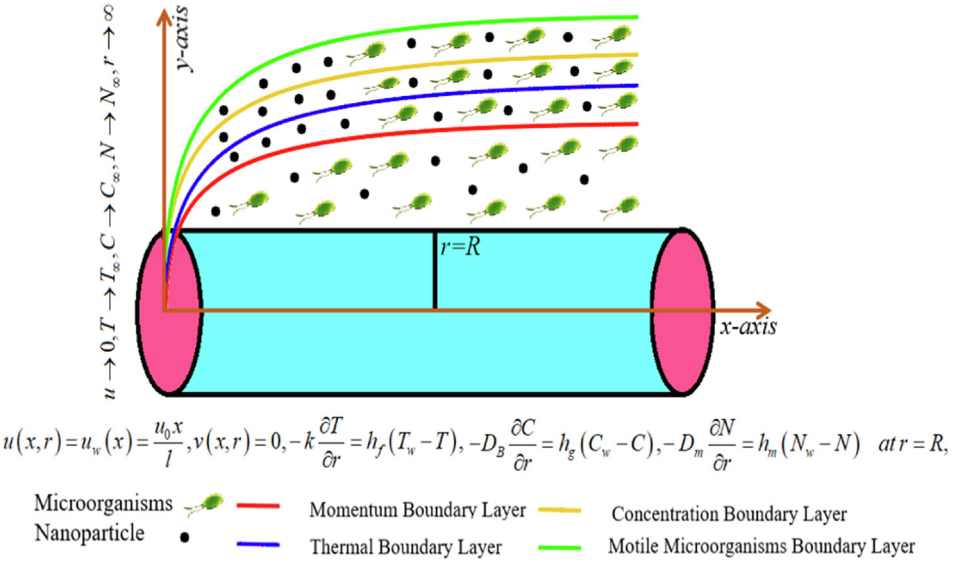

Fig. 1 Physical behavior of the current fluid model.

$$\left.\begin{aligned} &u\left(=\tfrac{u_0 x}{l}f'\right),\quad v\left(=-\tfrac{R}{r}\sqrt{\tfrac{u_0 v}{l}}f\right),\quad \zeta\left(=\sqrt{\tfrac{u_0}{vl}}\left(\tfrac{r^2-R^2}{2R}\right)\right)\\ &\theta\left(=\tfrac{T-T_\infty}{T_w-T_\infty}\right),\qquad \phi\left(=\tfrac{C-C_\infty}{C_w-C_\infty}\right),\qquad \chi\left(=\tfrac{N-N_\infty}{N_w-N_\infty}\right)\end{aligned}\right\} \tag{8}$$

The results of governing PDEs by using similarity transformations in the form of ODEs

$$\left.\begin{aligned}&\left(1+\frac{1}{\beta}\right)(2af''+(1+2\alpha\zeta)f'')-f'^2+ff''-M^2(f')\\&\quad+\lambda(\theta-Nr\phi-Nc\chi)=0\end{aligned}\right\} \tag{9}$$

$$\left.\begin{aligned}&(1+2\alpha\zeta)(\theta\theta''+\theta')\in_1+2\alpha\in_1\theta\theta'+(1+2\alpha\zeta)\theta''\\&\quad+PrEc(1+2\alpha\zeta)\left(1+\tfrac{1}{\beta}\right)f''^2\\&\quad+2\alpha\theta'+\left[\{1+Rd(1+(\theta_w-1)\theta)^3\}(1+2\alpha\zeta)\theta'\right]\theta''\\&\quad+PrNb(1+2\alpha\zeta)\theta'\phi'\\&\quad+PrEcM^2f'^2+PrNt(1+2\alpha\zeta)\theta'^2\\&\quad+Pr(f\theta')+Q_p\theta+Q_Eexp(-n\zeta)=0,\end{aligned}\right\} \tag{10}$$

$$\left.\begin{aligned}&(1+2\alpha\zeta)(\phi\phi''+\phi\prime)\in_2+2\alpha\in_2\phi\phi'\\&\quad+(1+2\alpha\zeta)\left(\phi''+\tfrac{Nt}{Nb}\theta''\right)+2\alpha\left(\phi'+\tfrac{Nt}{Nb}\theta'\right)\\&\qquad+\mathrm{Pr}Le(f\phi\prime)=0\end{aligned}\right\} \tag{11}$$

$$(1+2\alpha\zeta)\chi''+2\alpha\chi'+Lb(f\chi')-Pe[\phi''(\chi+\delta)+\chi'\phi']=0\} \tag{12}$$

With

$$\left.\begin{aligned}&f=0,\qquad f'=1,\qquad \theta'(\zeta)=-\lambda_1(1+\theta(\zeta)),\\&\phi'(\zeta)=-\lambda_2(1+\phi(\zeta)),\qquad \chi'(\zeta)=-\lambda_3(1+\chi(\zeta)),\\&\qquad\qquad \zeta\to 0\\&f'(\zeta)\to 0,\quad \theta(\zeta)\to 0,\quad \phi(\zeta)\to 0,\quad \chi(\zeta)\to 0,\ as\ \zeta\to\infty\end{aligned}\right\} \tag{13}$$

The dimensionless flow parameters are listed below:

Parameter Name	Parameter values
Curvature parameter	$\alpha\left(=\sqrt{\frac{vl}{u_0R^2}}\right)$
Mixed convection parameter	$\lambda\left(=\frac{(1-C_f)(T_f-T_\infty)\beta^*g^*}{z(u_0/l)^2}\right)$
Buoyancy-ratio parameter	$Nr\left(=\frac{(\rho_p-\rho_f)(C_f-C_\infty)}{\beta^*(1-C_f)(T_f-T_\infty)\rho_f}\right)$
Eckert parameter	$Ec\left(=\frac{u_w^2}{c_pT_\infty}\right)$
Bioconvective Rayleigh number	$Nc\left(=\frac{(\rho_m-\rho_f)(N_f-N_\infty)\gamma^{**}}{\beta^*(1-C_f)(T_f-T_\infty)\rho_f}\right)$
Magnetic parameter	$M^2\left(=\frac{\sigma B_0^2 l}{\rho u_0}\right)$
Brownian motion parameter	$Nb\left(=\frac{\tau D_B(C_w-C_0)}{v}\right)$
Temperature ratio parameter	$\theta_w\left(=\frac{T_w}{T_\infty}\right)$
Thermal radiation parameter	$Rd\left(=\frac{16\sigma^*T_\infty^3}{3kk^*}\right)$
Thermophoresis parameter	$Nt\left(=\frac{\tau D_T(T_w-T_0)}{vT_\infty}\right)$
Lewis number	$Le\left(=\frac{\alpha_f}{D_B}\right)$
Bioconvection Lewis parameter	$Lb\left(=\frac{v}{D_m}\right)$
Peclet number	$Pe\left(=\frac{bW_c}{D_m}\right)$
Microorganism difference	$\delta\left(=\frac{N_\infty}{N_w-N_0}\right)$
Thermal-Biot number	$\lambda_1\left(=h_f\sqrt{\frac{vl}{u_0}}\right)$
Solutal-Biot number	$\lambda_2\left(=h_g\sqrt{\frac{vl}{u_0}}\right)$
Microorganisms-Biot number	$\lambda_3\left(=h_n\sqrt{\frac{vl}{u_0}}\right)$

The main physical engineering parameters are addressed as:

$$\left.\begin{aligned}&C_f=\frac{2\tau_w}{\rho u_w^2},\ Nu_x=\frac{xq_w}{k(T-T_\infty)},Sh_x=\frac{xq_m}{D_B(C-C_\infty)},\\&Nn_x=\frac{xq_n}{D_m(N-N_\infty)}\end{aligned}\right\}, \tag{14}$$

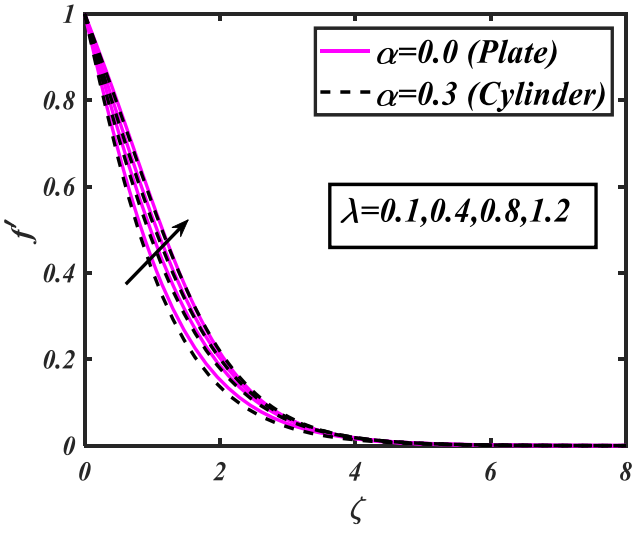

Fig. 2 Action of (λ) for(f').

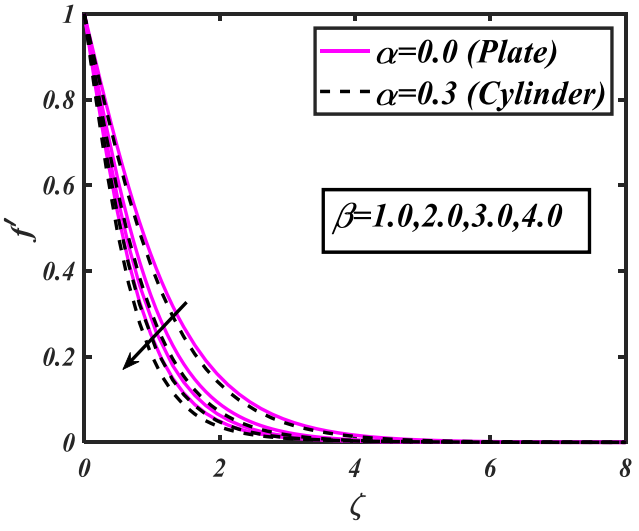

Fig. 3 Action of (β) for(f').

The shear stresses in the direction of the *x-axis* and *r-axis* are written as:

$$\left.\begin{aligned} \tau_w &= \mu\left(1+\frac{1}{\beta}\right)\left(\frac{\partial u}{\partial r}\right)_{r=R},\ q_w = -k\left(\frac{\partial T}{\partial r}\right)_{r=R}, \\ q_m &= -D_B\left(\frac{\partial C}{\partial r}\right)_{r=R},\ q_n = -D_m\left(\frac{\partial N}{\partial r}\right)_{r=R} \end{aligned}\right\}, \tag{15}$$

The dimensionless results of engineering quantities are:

$$\left.\begin{aligned} \tfrac{1}{2}C_f Re_x^{1/2} &= \left(1+\tfrac{1}{\beta}\right)f''(0),\ NuRe_x^{-1/2} = \lambda_1\left(1+\tfrac{1}{\theta(0)}\right), \\ ShRe_x^{-1/2} &= \lambda_2\left(1+\tfrac{1}{\phi(0)}\right), \\ NnRe_x^{-1/2} &= \lambda_3\left(1+\tfrac{1}{\chi(0)}\right) \end{aligned}\right\}, \tag{16}$$

3. Numerical scheme

In this research investigation, we analyze the impacts of the Bioconvectional flow of Casson nanofluid over a cylinder/-plate. The governing ordinary differential equations (9–12) with suitable boundary constraints (13) are computed numerically with the help of Bvp4c (Shampine et al. (Shampine et al., 2000) and Wang et al. (Wang et al., 2020) solver in Matlab by using the shooting approach with convergence rate10^{-6}. First, we convert the main differential equations system to the 1st-order ODEs model. The shooting approach is used to iteratively estimate the missing starting restrictions until the constraints are fulfilled. By providing new variables, the higher-order differential system of equations is reduced to the first order. The following ranges of the verses flow parameters for the formulation of figures are computed as $0.1 \leqslant \lambda \leqslant 1.2$ $1.0 \leqslant \beta \leqslant 4.0$ $0.1 \leqslant Nc \leqslant 1.2$ $0.1 \leqslant Nr \leqslant 1.2$ $0.1 \leqslant M \leqslant 1.2$

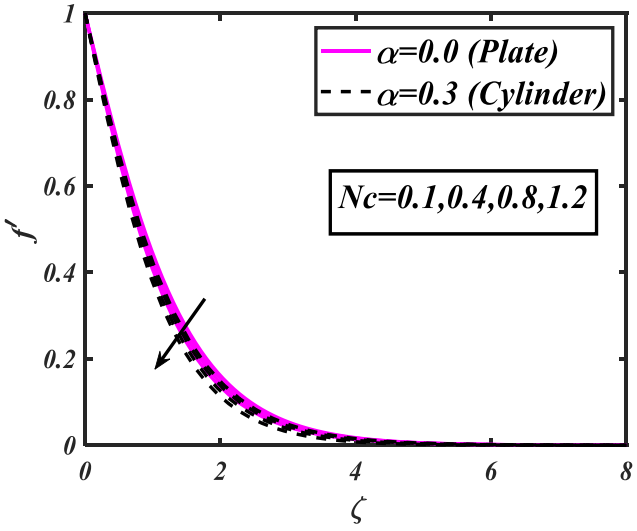

Fig. 4 Action of (Nc) for(f').

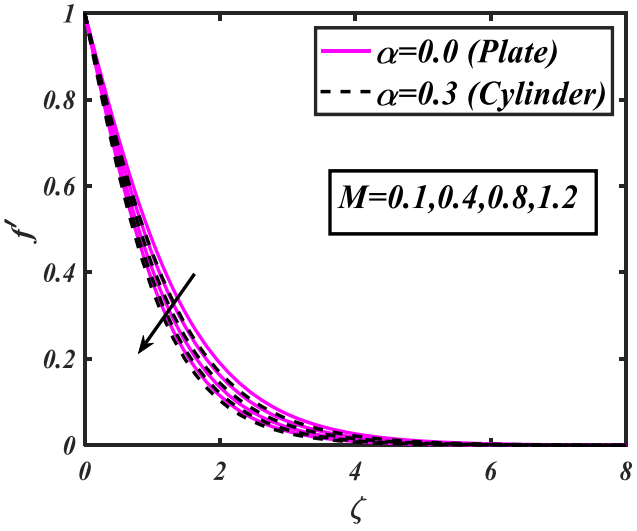

Fig. 6 Action of (M) for(f').

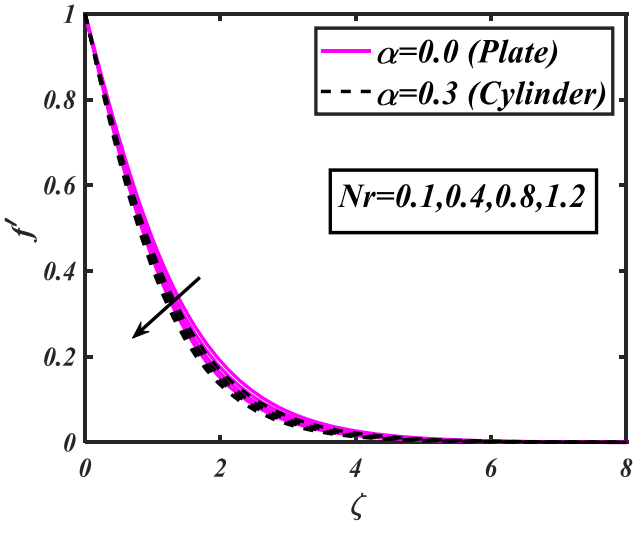

Fig. 5 Action of (Nr) for(f').

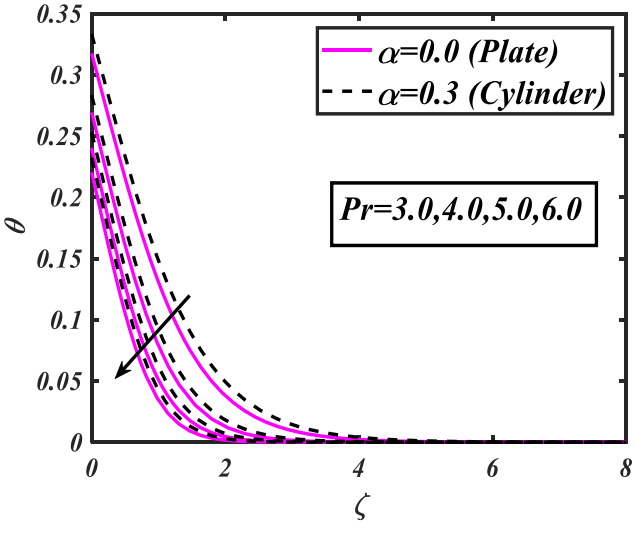

Fig. 7 Action of (Pr) for(θ).

$3.0 \leqslant \mathrm{Pr} \leqslant 6.0 \quad 1.5 \leqslant \theta_w \leqslant 1.80.1 \leqslant \lambda_1 \leqslant 0.40.1 \leqslant Q_E \leqslant 1.2$ $1.0 \leqslant Q_P \leqslant 1.9 \quad 1.0 \leqslant \in_1 \leqslant 4.0 \quad 0.1 \leqslant Nb \leqslant 0.25 \quad 0.1 \leqslant Nt \leqslant 0.41.2 \leqslant Le \leqslant 2.4 \quad 0.2 \leqslant \lambda_2 \leqslant 0.5 \quad 0.1 \leqslant \in_2 \leqslant 0.7 \quad 0.1 \leqslant \lambda_3 \leqslant 0.40.1 \leqslant Rd \leqslant 1.20.1 \leqslant Pe \leqslant 1.2$ and $1.2 \leqslant Lb \leqslant 2.4$ are analyzed.

Let

$$\left.\begin{aligned} f = h_1, f' = h_2, f'' = h_3, f''' = h_3', \theta = h_4, \theta' = h_5, \theta'' = h_5', \\ = h_6, \phi' = h_7, \phi'' = h_7', \qquad \chi = h_8, \chi' = h_9, \chi'' = h_9' \end{aligned}\right\}, \tag{17}$$

$$h_3' = \left.\frac{\left(1+\frac{1}{\beta}\right)(2\alpha h_3) - h_1 h_3 + h_2^2 + M^2(h_2) - \lambda(h_4 - Nrh_6 - Nch_8)}{\left(1+\frac{1}{\beta}\right)(1+2\alpha\zeta)}\right\}, \tag{18}$$

$$h_5' = \left.\frac{\begin{array}{c} -(1+2\alpha\zeta)(h_5)\in_1 - 2\alpha h_5 - \mathrm{Pr}Ec(1+2\alpha\zeta)\left(1+\frac{1}{\beta}\right)h_3^2 - \mathrm{Pr}Nb(1+2\alpha\zeta)h_5 h_7 \\ -2\alpha\in_1 h_4 h_5 - \mathrm{Pr}EcM^2 h_2^2 - \mathrm{Pr}Nt(1+2\alpha\zeta)h_5^2 - \mathrm{Pr}(h_1 h_5) - Q_p h_4 - Q_E \exp(-n\zeta), \end{array}}{(1+2\alpha\zeta)\left(h_4\in_1 + 1 + \left[\left\{1 + Rd(1+(\theta_w-1)h_4)^3\right\}h_5\right]\right)}\right\}, \tag{19}$$

$$h_7' = \left.\frac{(1+2\alpha\zeta)h_7\in_2 + 2\alpha\in_2 h_6 h_7 + \left(\begin{matrix}1+\\ 2\alpha\zeta\end{matrix}\right)\left(\frac{Nt}{Nb}h_5'\right) + 2\alpha\left(h_7 + \frac{Nt}{Nb}h_5\right) + \mathrm{Pr}Le(h_1 h_7)}{(1+2\alpha\zeta)(1+\in_2 h_6)}\right\}, \tag{20}$$

$$h_9' = \left.\frac{-2\alpha h_9 - Lb(h_1 h_9) + Pe\left[h_7'(h_8+\delta) + h_9 h_7\right]}{(1+2\alpha\zeta)}\right\}, \tag{21}$$

With

$$\left.\begin{aligned} h_1 = 0, h_2 = 1, h_5(\zeta) = -\lambda_1(1+h_4(\zeta)),\ h_7(\zeta) = -\lambda_2(1+h_6\phi(\zeta)), \\ h_9(\zeta) = -\lambda_3(h_8(\zeta)+1), \qquad \zeta \to 0 \\ h_8(\zeta) \to 0,\ \ h_6(\zeta) \to 0,\ \ h_4(\zeta) \to 0,\ \ h_2(\zeta) \to 0\ \ as\ \zeta \to \infty. \end{aligned}\right\}, \tag{22}$$

4. Results and Discussions:

Here, in this topic graphical and tabular data are utilized to scrutinize the impacts of the number of physical flow variables of the whole model due to using a scientific approach in the computational tool MATLAB. This work illustrates the Bio-convectional flow of Casson nanofluid with swimming motile microorganisms and heat source/sink passing through a cylinder/plate. The consequences of thermos-phoresis and Brownian motion effect for the current study in the MHD flow system are also discussed.

The consequence of the (λ) profile (f') is visualized in Fig. 2. The velocity field (f') boosted above the bottom level for the higher magnitude of mixed convection parameter(λ). Mixed convection variable measures the effect of free convection on flowing fluid in comparison to that of forced convection. The significance of the fluid parameter (β) (f') is depicted in

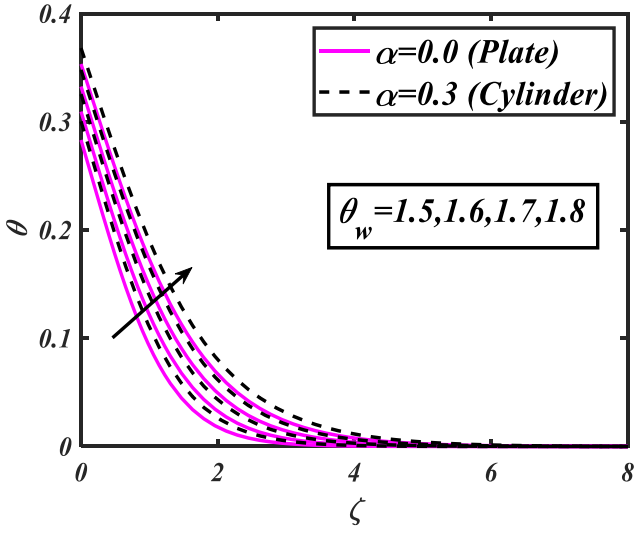

Fig. 8 Action of (θ_w) for(θ).

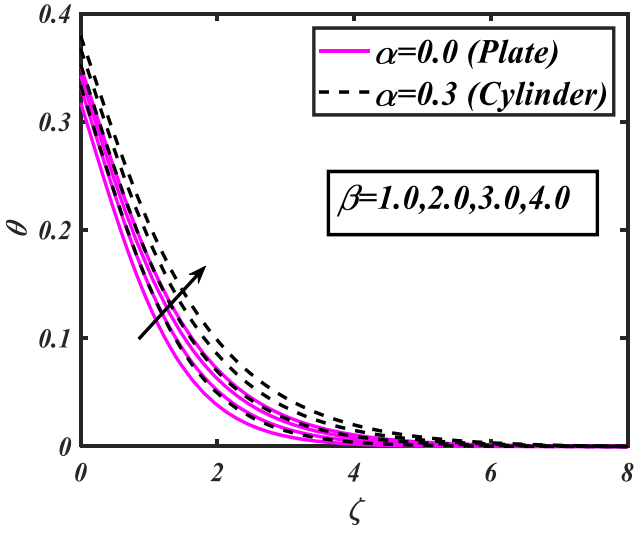

Fig. 9 Action of (β) for(θ).

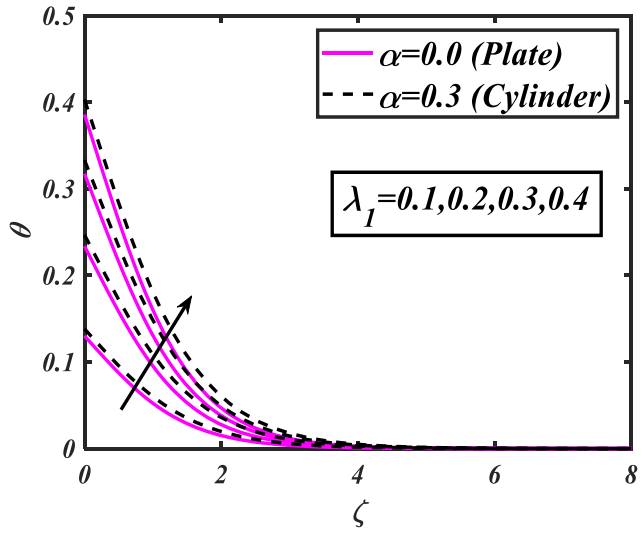

Fig. 10 Action of (λ_1) for(θ).

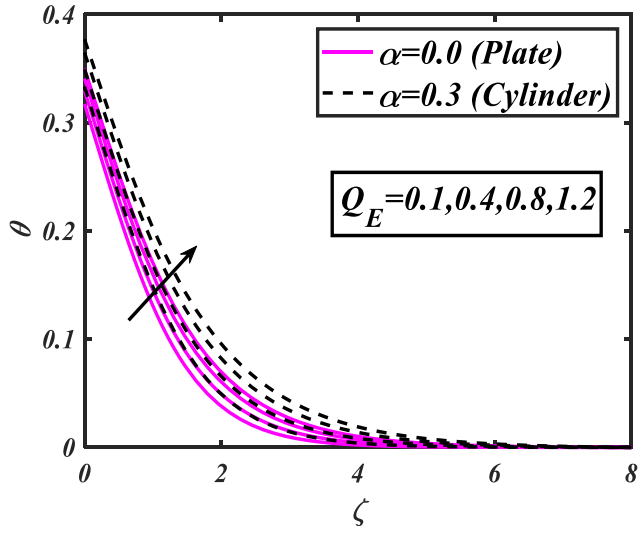

Fig. 11 Action of (Q_E) for(θ).

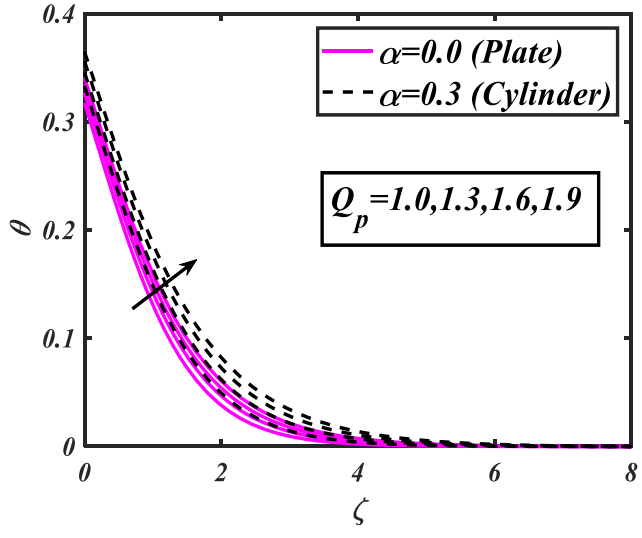

Fig. 12 Action of (Q_P) for(θ).

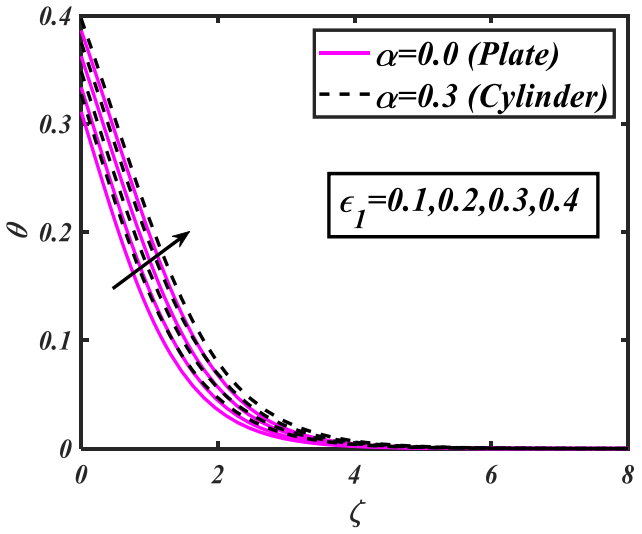

Fig. 13 Action of (ϵ_1) for(θ).

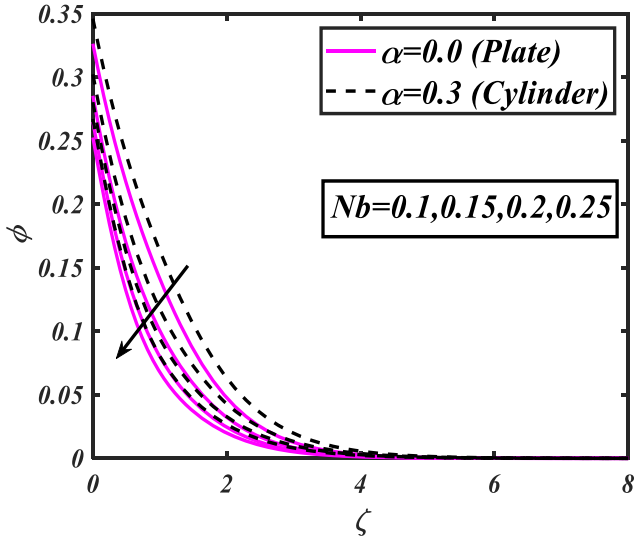

Fig. 14 Action of (Nb) for(ϕ).

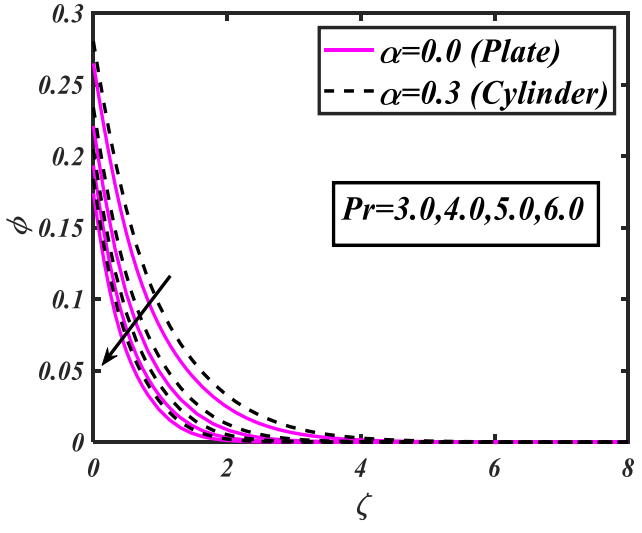

Fig. 15 Action of (Pr) for(ϕ).

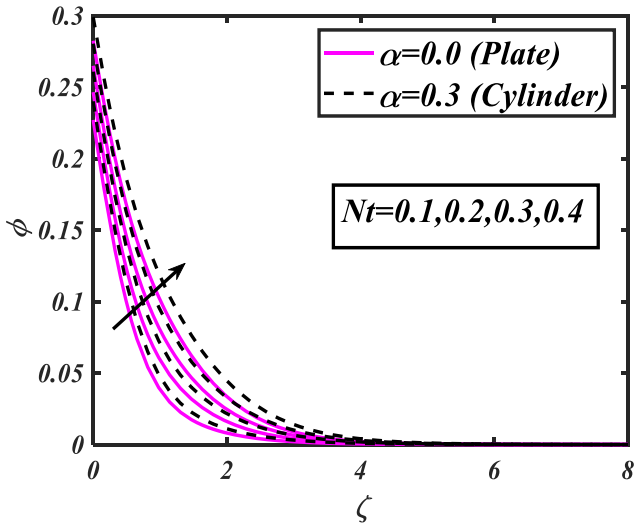

Fig. 16 Action of (Nt) for(ϕ).

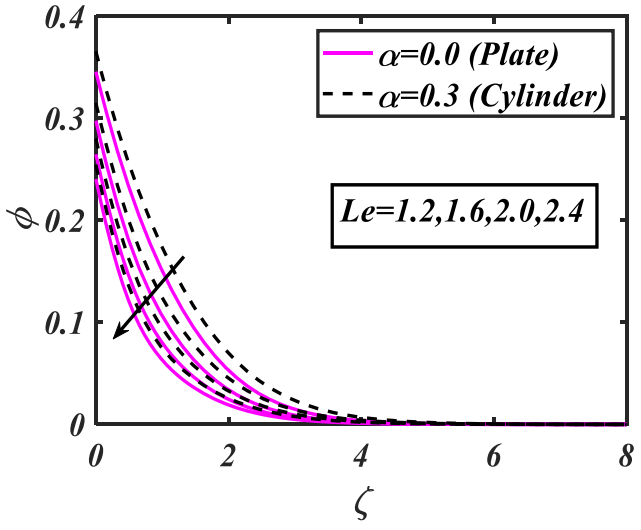

Fig. 17 Action of (Le) for(ϕ).

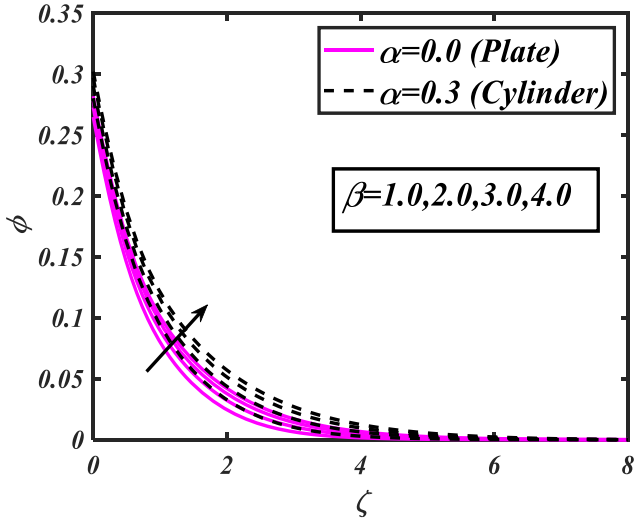

Fig. 18 Action of (β) for(ϕ).

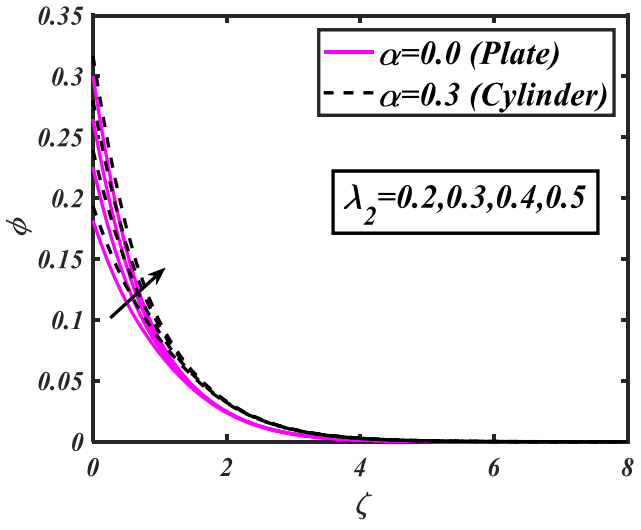

Fig. 19 Action of (λ_2) for(ϕ).

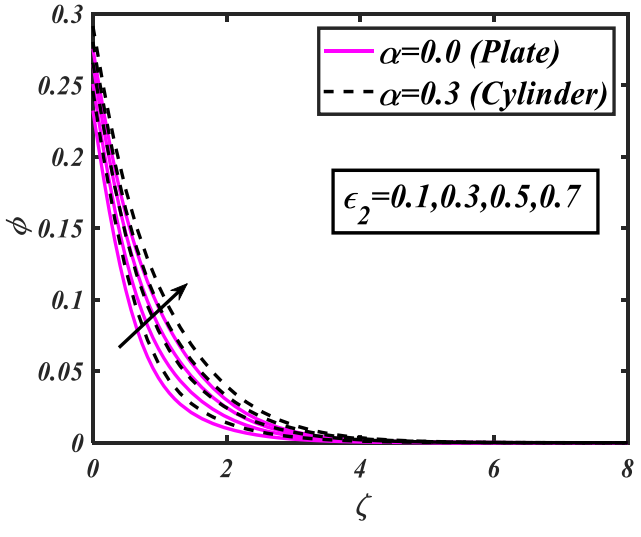

Fig. 20 Action of ($\in_2$) for(ϕ).

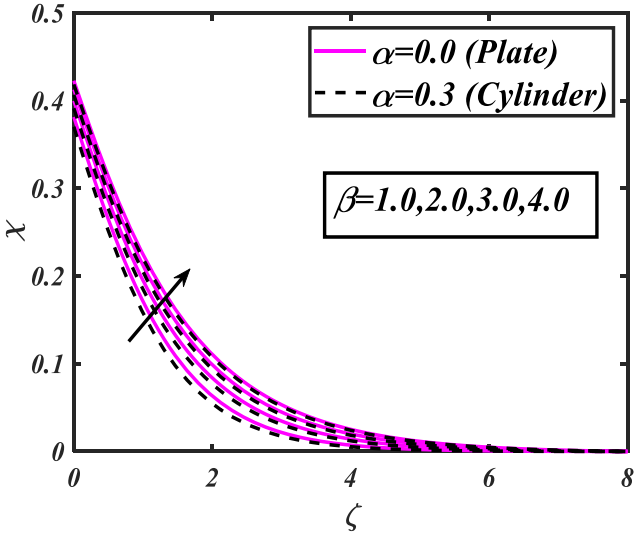

Fig. 21 Action of (β) for(χ).

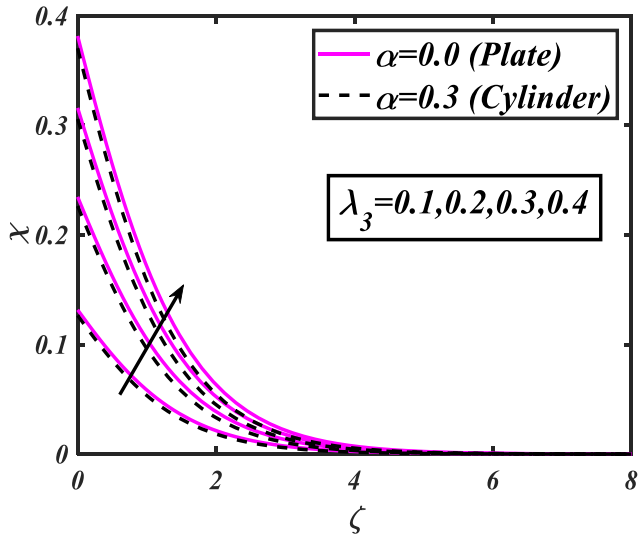

Fig. 22 Action of (λ_3) for(χ).

Fig. 3**.** The flow field (f') decreased for the increasing values of(β). The importance of the bioconvection Rayleigh parameter (Nc) for (f') displayed in Fig. 4. Incrementing magnitudes of bioconvection Rayleigh variable (Nc) declined velocity field of problem. The effect of the buoyancy ratio parameter (Nr) for the velocity distribution profile (f') is sketched in Fig. 5. The growing values of the buoyancy ratio parameter (Nr) decay the velocity distribution profile(f'). Both quantities are physically connected to buoyancy ratio forces that impede the flow of the two fluids. Fig. 6 shows the importance of (M) versus the velocity distribution profile is explained**.** The flow profile declined for the growing variations of the magnetic parameter. Physically, the changed magnetic parameter strengthens the external electrical field, which causes the velocity of the fluid to rise. Fig. 7 depicts the significance (Pr) of the thermal distribution profile(θ). The thermal distribution profile (θ) decays due to the mounting variation given(Pr). The Prandtl number depicts the thermal conductivity to thermal diffusivity ratio. As a result, an increased Prandtl number leads to decreased thermal diffusivity. As a result, as the Prandtl number increases, the (θ) decreases. The consequence of (θ_w) the temperature distribution field (θ) is plotted in Fig. 8. The (θ) increased for higher values for the temperature ratio parameter(θ_w). Physically, enhancing the non-linear thermal radiation parameter raises internal energy. As a consequence, the thermal field is enhanced. Fig. 9displaysthe aspect of (β) the temperature distribution field(θ). The temperature distribution field (θ) is augmented by growing valuations of the Casson fluid parameter(β). Fig. 10 outlined the outcomes due to temporal stratification (λ_1) Biot number on the thermal field(θ). The increasing counts of temporal stratification (λ_1) Biot number increased the thermal field(θ). Fig. 11 is noted the behavior of the exponential heat-sink parameter (Q_E) for the thermal distribution profile(θ). The thermal distribution profile (θ) boomed due to the increasing counts exponential thermal-sink variable(Q_E). The attitude of (Q_P) the temperature field (θ) considered in Fig. 12**.** The rising magnitude of the thermal-source variable (Q_P) enhances the thermal distribution profile(θ). Fig. 13p or **traysresults** of the thermal conductivity count $(\in_1)$ on the thermal distribution field(θ). The increasing evaluation of $(\in_1)$ enhanced the temperature(θ). Fig. 14described the (Nb) for(ϕ). The concentration distribution field (ϕ) reduces by the advancement in magnitude in favor of the Brownian motion variable(Nb). Fig. 15disclosed consequences of the Prandtl count Pr for the concentration distribution profile(ϕ). It has seemed that the escalating approximation of Prandtlcount decays the concentration distribution profile(ϕ). Actuality, the connection between Pr and thermal diffusivity is inverse. An increase in Pr generates reduced thermal diffusivity, resulting in a decrease in the curves. The nature of (Nt) regarding concentration distribution field (ϕ) is detailed in Fig. 16. The concentration distribu-

Table 1 Numerical results of local skin friction coefficient $-f''(0)$ for diverse parameters.

Parameters						$-f''(0)$	
M	λ	Nr	Nc	Ec	β	$\alpha = 0.0$	$\alpha = 0.3$
0.4	0.2	0.1	0.5	0.3	0.1	**0.6502**	**0.6945**
0.8						**0.7063**	**0.7465**
1.2						**0.7547**	**0.7915**
0.5	**0.5**	0.1	0.5	0.3	0.1	**0.6555**	**0.6925**
	1.0					**0.6398**	**0.6551**
	2.0					**0.6091**	**0.6321**
0.5	0.2	**0.2**	0.5	0.3	0.1	**0.6656**	**0.7089**
		1.5				**0.6720**	**0.7161**
		2.5				**0.6769**	**0.7217**
0.5	0.2	0.1	**0.1**	0.3	0.1	**0.6646**	**0.7089**
			0.8			**0.6780**	**0.7151**
			1.4			**0.6799**	**0.7237**
0.5	0.2	0.1	0.5	**0.5**	0.1	**0.6649**	**0.7797**
				1.0		**0.6754**	**0.7935**
				1.5		**0.6869**	**0.9170**
0.5	0.2	0.1	0.5	0.3	**0.4**	**0.6566**	**0.6989**
					0.8	**0.6640**	**0.7063**
					1.2	**0.6789**	**0.7257**

tion profile (ϕ) incremented for an increased evaluation of the thermophoresis parameter(Nt). The thermophoresis effect is the transfer force that happens when a temperature gradient exists. The effect of Lewis number (Le) for the concentration distribution field (ϕ) is elucidated in Fig. 17. The concentration distribution field (ϕ) is declined for growing valuations

Table 2 Numericresults of $-\theta'(0)$ local Nusselt number for diverse variables.

Variables								$-\theta'(0)$	
M	λ	Nr	Nc	Pr	Nt	Rd	λ_1	$\alpha = 0.0$	$\alpha = 0.3$
0.4	0.2	0.1	0.5	2.0	0.3	0.5	0.3	**0.2051**	**0.2004**
0.8								**0.2038**	**0.1990**
1.2								**0.2025**	**0.1977**
0.5	**0.1**	0.1	0.5	2.0	0.3	0.5	0.3	**0.2050**	**0.1935**
	0.8							**0.2052**	**0.2051**
	1.4							**0.2060**	**0.2058**
0.5	0.2	**0.2**	0.5	2.0	0.3	0.5	0.3	**0.2048**	**0.2000**
		1.5						**0.2046**	**0.1998**
		2.5						**0.2045**	**0.1997**
0.5	0.2	0.1	**0.1**	2.0	0.3	0.5	0.3	**0.2055**	**0.2003**
			0.8					**0.2046**	**0.1999**
			1.4					**0.2035**	**0.1998**
0.5	0.2	0.1	0.5	**3.0**	0.3	0.5	0.3	**0.2192**	**0.2150**
				4.0				**0.2280**	**0.2241**
				5.0				**0.2329**	**0.2303**
0.5	0.2	0.1	0.5	2.0	**0.5**	0.5	0.3	**0.2019**	**0.1968**
					0.8			**0.1974**	**0.1918**
					1.4			**0.1875**	**0.1808**
0.5	0.2	0.1	0.5	2.0	0.3	**0.6**	0.3	**0.1925**	**0.1978**
						1.2		**0.1902**	**0.1858**
						1.8		**0.1759**	**0.1759**
0.5	0.2	0.1	0.5	2.0	0.3	0.5	**0.8**	**0.2795**	**0.2731**
							1.6	**0.2714**	**0.2651**
							2.4	**0.2680**	**0.2618**

Table 3 Numeric results of $-\phi'(0)$ local Sherwood number for diverse variables.

Variables								$-\phi'(0)$	
M	λ	Nr	Le	Pr	Nt	Nb	λ_2	$\alpha = 0.0$	$\alpha = 0.3$
0.4	0.2	0.1	2.0	2.0	0.3	0.2	0.4	**0.2943**	**0.2881**
0.8								**0.2933**	**0.2871**
1.2								**0.2924**	**0.2861**
0.5	**0.1**	0.1	2.0	2.0	0.3	0.2	0.4	**0.2942**	**0.2878**
	0.8							**0.2945**	**0.2912**
	1.4							**0.2950**	**0.2945**
0.5	0.2	**0.2**	2.0	2.0	0.3	0.2	0.4	**0.2940**	**0.2878**
		1.5						**0.2939**	**0.2877**
		2.5						**0.2938**	**0.2876**
0.5	0.2	0.1	**3.0**	2.0	0.3	0.2	0.4	**0.3145**	**0.3095**
			4.0					**0.3266**	**0.3223**
			5.0					**0.3348**	**0.3310**
0.5	0.2	0.1	2.0	**3.0**	0.3	0.2	0.4	**0.3115**	**0.3064**
				4.0				**0.3226**	**0.3181**
				5.0				**0.3304**	**0.3264**
0.5	0.2	0.1	2.0	2.0	**0.5**	0.2	0.4	**0.2735**	**0.2804**
					0.8			**0.2551**	**0.2630**
					1.4			**0.2305**	**0.2389**
0.5	0.2	0.1	2.0	2.0	0.3	**0.5**	0.4	**0.3088**	**0.3037**
						0.8		**0.3125**	**0.3076**
						1.4		**0.3152**	**0.3105**
0.5	0.2	0.1	2.0	2.0	0.3	0.5	**0.8**	**0.2032**	**0.1983**
							1.6	**0.2011**	**0.1961**
							2.4	**0.1999**	**0.1948**

Table 4 Numerical results of local microorganism density number $-\chi'(0)$ for diverse parameters.

Parameters						$-\chi'(0)$	
M	λ	Nr	Pe	Lb	λ_3	$\alpha = 0.0$	$\alpha = 0.3$
0.4	0.2	0.1	0.1	2.0	0.4	**0.2849**	**0.2890**
0.8						**0.2835**	**0.2878**
1.2						**0.2823**	**0.2867**
0.5	**0.5**	0.1	0.1	2.0	0.4	**0.2848**	**0.2866**
	1.0					**0.2851**	**0.2872**
	2.0					**0.2857**	**0.2875**
0.5	0.2	**0.2**	0.1	2.0	0.4	**0.2845**	**0.2887**
		1.5				**0.2844**	**0.2887**
		2.5				**0.2843**	**0.2886**
0.5	0.2	0.1	**0.4**	2.0	0.4	**0.2916**	**0.2944**
			0.8			**0.3000**	**0.301**
			1.2			**0.3076**	**0.3078**
0.5	0.2	0.1	0.1	**3.0**	0.4	**0.3027**	**0.3064**
				4.0		**0.3140**	**0.3175**
				5.0		**0.3220**	**0.3253**
0.5	0.2	0.1	0.1	2.0	**0.8**	**0.3051**	**0.3067**
					1.6	**0.2915**	**0.3029**
					2.4	**0.2855**	**0.2978**

of Lewis number(Le). The mass diffusion and thermal conductivity of a fluid are linked by the Lewis number. Fig. 18designates the result of (β) for the concentration distribution field(ϕ). The concentration field is augmented by the rising valuation of the(β). Fig. 19showsthe outcomes of the Solutal-Biot number (λ_2) against the concentration distribution field(ϕ). The concentration distribution field (ϕ) increased with mounting values of the Solutal-Biot number(λ_2). Fig. 20founds the characteristics of thermal diffusivity ($\in_2$) for the concentration distribution field(ϕ). The concentration distribution field (ϕ) reduced with the increasing values of thermal diffusivity($\in_2$). The effect (β) on the microorganism field (χ) is designed in Fig. 21. The microorganism field (χ) is enhanced by intensifying values of the Casson fluid parameter(β). Importance of motile microorganisms Biot number (λ_3) on microorganism field (χ) is delineated in Fig. 22**.** The (χ) increase with increasing estimations of microorganisms' Biot number(λ_3).

5. Figures

See Figs. 2-22.

6. Tabular values

Table 1 depicts that skin friction is increased by the growing counts of the buoyancy ratio variable (Nr) and bioconvection Rayleigh variable (Nc) while decreased for the mixed convection parameter(λ). Table 2 reveals that the local Nusselt-number is reduced for the variation of thermal radiation parameter (Rd) and thermal Biot number(λ_1). Table 3 analyzed that the local Sherwood number is decreased for the magnetic parameter(M). Table 4 examined that the local motile microorganism density number is upgraded for bioconvection Lewis number (Lb) and Peclet number(Pe). Table 5 compares the results with Tamoor et al. (Song et al., 2021) and Fang et al. (Shampine et al., 2000) for various values of the magnetic parameter. These findings were determined to be in good agreement. Table 6 compares Nusselt number values with those reported in the literature. We discovered a great match, which verifies the current findings.

Table 5 Comparison of $-f''(0)$ for dissimilar values of magnetic parameter$M$.

M	Fang et al. (Fang et al., 2009)	Tamoor et al. (Tamoor et al., 2017)	Current work
0.0	1.0000	1.00000	1.00000
0.2	1.0198	1.01980	1.01981
0.5	1.1180	1.11803	1.11804
0.8	1.2806	1.28063	1.28064
1.0	1.4142	1.41421	1.41422

Table 6 Comparison of $-\theta'(0)$ regarding dissimilar counts of Prandtl countPr.

Pr	Rehman et al. (Rehman et al., 2022)	Mukhopadhyay (Mukhopadhyay, 2013)	Current work
1.0	0.9544	0.9547	0.9549
3.0	1.4702	1.4714	1.4715
5.0	1.8952	1.8961	1.8963

7. Conclusions

We investigated the two-dimensional stream of Casson nano-fluid across cylinder/plate including non-linear thermal radiation, exponential thermal source/sink, motile microorganisms, and bioconvection. Brownian motion and the thermophoresis phenomenon are also looked into. The similarity transformations are used to turn the governing (PDEs) into a non-linear ODE system. The transformed ODEs are then numerically resolved in MATLAB computational software

using the Bvp4c solver (shooting technique). The graphical and tabular results demonstrate the effect of including physiological parameters. The significant findings are:

- The velocity distribution profile declined regarding the increasing rates of the Casson fluid parameter and bioconvective Rayleigh variables.
- The velocity distribution field is enhanced regarding the higher magnitude of mixed convection parameter while declining for buoyancy-ratio number.
- The enhancement in the values of the temperature ratio parameter, thermal Biot number, and Casson fluid parameter causes an important increase in the temperature profile.
- The augmentation in the magnitude of the Prandtl number causes a significant decline in the temperature distribution profile while enhanced for the Solutal Biot number.
- The concentration distribution profile is improved with an improvement in the values of the Solutal Biot number, and Casson fluid parameter while decreased for the Lewis number.
- The microorganism profile is raised by raising the magnitude of microorganisms-Biotparameter and Casson nanofluid parameter.
- The currently studied bioconvective nanofluid is used in different engineering and technological applications like gas turbines, automobile radiators, heat exchangers, microbial fuel cells, nuclear reactors, and bio-medical utilizations.

Declaration of Competing Interest

The authors declare that they have no known competing financial interests or personal relationships that could have appeared to influence the work reported in this paper.

References

Abbas, N., Rehman, K.U., Shatanawi, W., Abodayeh, K., 2022. Mathematical model of temperature-dependent flow of power-law nanofluid over a variable stretching Riga sheet. Waves Random Complex Media, 1–18.

Abbas, N., Shatanawi, W., 2022. Theoretical Survey of Time-Dependent Micropolar Nanofluid Flow over a Linear Curved Stretching Surface. Symmetry 14 (8), 1629.

Abbas, N., Shatanawi, W., 2022. Heat and mass transfer of micropolar-casson nanofluid over vertical variable stretching riga sheet. Energies 15 (14), 4945.

Ali, A., Farooq, H., Abbas, Z., Bukhari, Z., Fatima, A., 2020. Impact of Lorentz force on the pulsatile flow of a non-Newtonian Casson fluid in a constricted channel using Darcy's law: a numerical study. Sci. Rep. 10 (1), 1–15.

Ali, F., Khan, N., Imtiaz, A., Khan, I., Sheikh, N.A., 2019. The impact of magnetohydrodynamics and heat transfer on the unsteady flow of Casson fluid in an oscillating cylinder via integral transform: A Caputo-Fabrizio fractional model. Pramana 93 (3), 1–12.

Ali, A., Sarkar, S., Das, S., Jana, R.N., 2022. A report on entropy generation and Arrhenius kinetics in magneto-bioconvective flow of Cross nanofluid over a cylinder with wall slip. Int. J. Ambient Energy, 1–16.

Ali, A., Sarkar, S., Das, S., 2023. Bioconvective chemically reactive entropy optimized Cross-nano-material conveying oxytactic microorganisms over a flexible cylinder with Lorentz force and Arrhenius kinetics. Math. Comput. Simul 205, 1029–1051.

Alizadeh, R., Gomari, S.R., Alizadeh, A., Karimi, N., Li, L.K., 2021. Combined heat and mass transfer and thermodynamic irreversibilities in the stagnation-point flow of Casson rheological fluid over a cylinder with catalytic reactions and inside a porous medium under local thermal nonequilibrium. Comput. Math. Appl. 81, 786–810.

Anantha Kumar, K., Sugunamma, V., Sandeep, N., 2020. Effect of thermal radiation on MHD Casson fluid flow over an exponentially stretching curved sheet. J. Therm. Anal. Calorim. 140 (5), 2377–2385.

Ayodeji, F., Tope, A., Pele, O., 2020. Magneto-hydrodynamics (MHD) Bioconvection nanofluid slip flow over a stretching sheet with thermophoresis, viscous dissipation and brownian motion. Mach. Learn. Res 4 (4), 51.

Azam, M., Xu, T., Nayak, M.K., Khan, W.A., Khan, M., 2022. Gyrotactic microorganisms and viscous dissipation features on radiative Casson nanoliquid over a moving cylinder with activation energy. Waves Random Complex Media, 1–23.

Bhattacharyya, K., Uddin, M.S., Layek, G.C., 2016. Exact solution for thermal boundary layer in Casson fluid flow over permeable shrinking sheet with variable wall temperature and thermal radiation. Alex. Eng. J. 55 (2), 1703–1712.

Bhatti, M.M., Michaelides, E.E., 2021. Study of Arrhenius activation energy on the thermo-bioconvection nanofluid flow over a Riga plate. J. Therm. Anal. Calorim. 143 (3), 2029–2038.

Bhatti, M.M., Shahid, A., Abbas, T., Alamri, S.Z., Ellahi, R., 2020. Study of activation energy on the movement of gyrotactic microorganism in a magnetized nanofluids past a porous plate. Processes 8 (3), 328.

Bhatti, M.M., Bég, O.A., Ellahi, R., Abbas, T., 2022. Natural convection non-Newtonian EMHD dissipative flow through a microchannel containing a non-Darcy porous medium: Homotopy perturbation method study. Qualitative Theory of Dynamical Systems 21 (4), 1–27.

Buongiorno, J., 2006. Convective transport in nanofluids. J. Heat Transf. 128 (3), 240–250.

Cao, W., Animasaun, I.L., Yook, S.J., Oladipupo, V.A., Ji, X., 2022. Simulation of the dynamics of colloidal mixture of water with various nanoparticles at different levels of partial slip: Ternary-hybrid nanofluid. Int. Commun. Heat Mass Transfer 135, 106069.

Choi, S.U.S., Singer, D.A., Wang, H.P., 1995. Developments and applications of non-Newtonian flows. ASME Fed. 66, 99–105.

Fang, T., Zhang, J., Yao, S., 2009. Slip MHD viscous flow over a stretching sheet–an exact solution. Commun. Nonlinear Sci. Numer. Simul. 14 (11), 3731–3737.

Gireesha, B.J., Sindhu, S., 2020. MHD natural convection flow of Casson fluid in an annular microchannel containing porous medium with heat generation/absorption. Nonlinear Engineering 9 (1), 223–232.

Haldar, S., Mukhopadhyay, S., Layek, G.C., 2017. Dual solutions of Casson fluid flows over a power-law stretching sheet. J. Appl. Mech. Tech. Phys. 58 (4), 629–634.

Hiremath, A., Basha, H., Kethireddy, B., Reddy, G.J., Narayanan, N. S., 2019. The effect of thermal expansion coefficient on unsteady non-Newtonian supercritical Casson fluid flow past a vertical cylinder. Pramana 93 (2), 1–16.

Hussain, A., Afzal, S., Rizwana, R., Malik, M.Y., 2020. MHD stagnation point flow of a Casson fluid with variable viscosity flowing past an extending/shrinking sheet with slip effects. Physica A 553, 124080.

Khan, N.S., Shah, Q., Bhaumik, A., Kumam, P., Thounthong, P., Amiri, I., 2020. Entropy generation in bioconvection nanofluid flow between two stretchable rotating disks. Sci. Rep. 10 (1), 1–26.

Krishna, M.V., 2020. Hall and ion slip impacts on unsteady MHD free convective rotating flow of Jeffreys fluid with ramped wall temperature. Int. Commun. Heat Mass Transfer 119, 104927.

Krishna, M.V., 2021. Hall and ion slip effects on radiative MHD rotating flow of Jeffreys fluid past an infinite vertical flat porous surface with ramped wall velocity and temperature. Int. Commun. Heat Mass Transfer 126, 105399.

Krishna, M.V., Swarnalathamma, B.V., Chamkha, A.J., 2019. Investigations of Soret, Joule and Hall effects on MHD rotating mixed convective flow past an infinite vertical porous plate. J. Ocean. Eng. Sci. 4 (3), 263–275.

Krishna, M.V., Ahamad, N.A., Chamkha, A.J., 2020. Hall and ion slip effects on unsteady MHD free convective rotating flow through a saturated porous medium over an exponential accelerated plate. Alex. Eng. J. 59 (2), 565–577.

Krishna, M.V., Chamkha, A.J., 2019. Hall and ion slip effects on MHD rotating boundary layer flow of nanofluid past an infinite vertical plate embedded in a porous medium. Results Phys. 15, 102652.

Krishna, M.V., Chamkha, A.J., 2020. Hall and ion slip effects on MHD rotating flow of elastico-viscous fluid through a porous medium. Int. Commun. Heat Mass Transfer 113, 104494.

Krishna, M.V., Chamkha, A.J., 2021. Hall and ion slip effects on magnetohydrodynamic convective rotating flow of Jeffreys fluid over an impulsively moving vertical plate embedded in a saturated porous medium with ramped wall temperature. Numer. Methods Partial Differential Equations 37 (3), 2150–2177.

Kumar, K.A., Sugunamma, V., Sandeep, N., Reddy, J.R., 2019. MHD stagnation point flow of Williamson and Casson fluids past an extended cylinder: a new heat flux model. SN Applied Sciences 1 (7), 705.

Kuznetsov, A.V., 2012. Nanofluid bioconvection: interaction of microorganisms oxytactic upswimming, nanoparticle distribution, and heating/cooling from below. Theor. Comput. Fluid Dyn. 26 (1), 291–310.

Lund, L.A., Omar, Z., Khan, I., Baleanu, D., Nisar, K.S., 2020. Dual similarity solutions of MHD stagnation point flow of Casson fluid with effect of thermal radiation and viscous dissipation: stability analysis. Sci. Rep. 10 (1), 1–13.

Muhammad, T., Alamri, S.Z., Waqas, H., Habib, D., Ellahi, R., 2021. Bioconvection flow of magnetized Carreau nanofluid under the influence of slip over a wedge with motile microorganisms. J. Therm. Anal. Calorim. 143 (2), 945–957.

Mukhopadhyay, S., 2013. MHD boundary layer flow and heat transfer over an exponentially stretching sheet embedded in a thermally stratified medium. Alex. Eng. J. 52 (3), 259–265.

Mukhopadhyay, S., Layek, G.C., Samad, S.A., 2005. Study of MHD boundary layer flow over a heated stretching sheet with variable viscosity. Int. J. Heat Mass Transf. 48 (21–22), 4460–4466.

Mukhopadhyay, S., De, P.R., Bhattacharyya, K., Layek, G.C., 2013. Casson fluid flow over an unsteady stretching surface. Ain Shams Eng. J. 4 (4), 933–938.

Murthy, M.K., Raju, C.S., Nagendramma, V., Shehzad, S.A., Chamkha, A.J., 2019. Magnetohydrodynamics boundary layer slipCasson fluid flow over a dissipated stretched cylinder.*Defect and Diffusion*. Forum 393, 73–82.

Qadan, H., Alkasasbeh, H., Yaseen, N., Sawalmeh, M.Z., ALKhalafat, S., 2019. A Theoretical study of steady MHD mixed convection heat transfer flow for a horizontal circular cylinder embedded in a micropolarcasson fluid with thermal radiation. Journal of Computational Applied Mechanics 50 (1), 165–173.

Reddy, G.J., Kethireddy, B., Kumar, M., Rani, H.P., 2019. Entropy generation for transient Casson fluid past a vertical cylinder with Bejan's flow visualization. Int. J. Comput. Methods Eng. Sci. Mech. 20 (3), 175–200.

Reddy, M.G., Kumari, P.V., Padma, P., 2018. Effect of thermal radiation on MHD casson nano fluid over a cylinder. Journal of Nanofluids 7 (3), 428–438.

Rehman, K.U., Shatanawi, W., Ashraf, S., Kousar, N., 2022. Numerical Analysis of Newtonian Heating Convective Flow by Way of Two Different Surfaces. Appl. Sci. 12 (5), 2383.

Salahuddin, T., Arshad, M., Siddique, N., Alqahtani, A.S., Malik, M. Y., 2020. Thermophyical properties and internal energy change in Casson fluid flow along with activation energy. Ain Shams Eng. J. 11 (4), 1355–1365.

Sarkar, S., Das, S., 2022. Magneto-thermo-bioconvection of a chemically sensitive Cross nanofluid with an infusion of gyrotactic microorganisms over a lubricious cylindrical surface: Statistical analysis. Int. J. Model. Simul., 1–22

Sarkar, S., Ali, A., & Das, S. 2022. Bioconvection in non-Newtonian nanofluid near a perforated Riga plate induced by haphazard motion of nanoparticles and gyrotactic microorganisms in the attendance of thermal radiation, and Arrhenius chemical reaction: Sensitivity analysis. International Journal of Ambient Energy, (just-accepted), 1-34.

Shahid, A., Huang, H., Bhatti, M.M., Zhang, L., Ellahi, R., 2020. Numerical investigation on the swimming of gyrotactic microorganisms in nanofluids through porous medium over a stretched surface. Mathematics 8 (3), 380.

Shampine, L.F., Kierzenka, J., Reichelt, M.W., 2000. Solving boundary value problems for ordinary differential equations in MATLAB with bvp4c. Tutorial notes 2000, 1–27.

Shankar, D.G., Raju, C.S.K., Kumar, M.J., Makinde, O.D., 2020. Cattaneo-Christov heat flux on an MHD 3D free convection Casson fluid flow over a stretching sheet. Eng. Trans. 68 (3), 223–238.

Shatnawi, T.A., Abbas, N., Shatanawi, W., 2022. Comparative study of Casson hybrid nanofluid models with induced magnetic radiative flow over a vertical permeable exponentially stretching sheet. AIMS Mathematics 7 (12), 20545–20564.

Shatnawi, T.A., Abbas, N., Shatanawi, W., 2022. Mathematical Analysis of Unsteady Stagnation Point Flow of Radiative Casson Hybrid Nanofluid Flow over a Vertical Riga Sheet. Mathematics 10 (19), 3573.

Shehzad, S.A., Reddy, M.G., Rauf, A., Abbas, Z., 2020. Bioconvection of Maxwell nanofluid under the influence of double diffusive Cattaneo-Christov theories over isolated rotating disk. Phys. Scr. 95, (4) 045207.

Sohail, M., Shah, Z., Tassaddiq, A., Kumam, P., Roy, P., 2020. Entropy generation in MHD Casson fluid flow with variable heat conductance and thermal conductivity over non-linear bi-directional stretching surface. Sci. Rep. 10 (1), 1–16.

Song, Y.Q., Obideyi, B.D., Shah, N.A., Animasaun, I.L., Mahrous, Y. M., Chung, J.D., 2021. Significance of haphazard motion and thermal migration of alumina and copper nanoparticles across the dynamics of water and ethylene glycol on a convectively heated surface. Case Studies in Thermal Engineering 26, 101050.

Tamoor, M., Waqas, M., Khan, M.I., Alsaedi, A., Hayat, T., 2017. Magnetohydrodynamic flow of Casson fluid over a stretching cylinder. Results Phys. 7, 498–502.

Thumma, T., Wakif, A., Animasaun, I.L., 2020. Generalized differential quadrature analysis of unsteady three-dimensional MHD radiating dissipative Casson fluid conveying tiny particles. Heat Transfer 49 (5), 2595–2626.

Tulu, A., Ibrahim, W., 2020. Spectral relaxation method analysis of Casson nanofluid flow over stretching cylinder with variable thermal conductivity and Cattaneo-Christov heat flux model. Heat Transfer 49 (6), 3433–3455.

Ullah, I., Alkanhal, T.A., Shafie, S., Nisar, K.S., Khan, I., Makinde, O.D., 2019. MHD slip flow of Casson fluid along a nonlinear permeable stretching cylinder saturated in a porous medium with chemical reaction, viscous dissipation, and heat generation/absorption. Symmetry 11 (4), 531.

Veera Krishna, M., Jyothi, K., Chamkha, A.J., 2018. Heat and mass transfer on unsteady, magnetohydrodynamic, oscillatory flow of second-grade fluid through a porous medium between two vertical plates, under the influence of fluctuating heat source/sink, and chemical reaction. Int. J. Fluid Mech. Res 45 (5), 459–477.

Venkata Ramudu, A.C., Anantha Kumar, K., Sugunamma, V., Sandeep, N., 2020. Influence of suction/injection on MHD Casson fluid flow over a vertical stretching surface. J. Therm. Anal. Calorim. 139 (6), 3675–3682.

Wang, J., Khan, W.A., Asghar, Z., Waqas, M., Ali, M., Irfan, M., 2020. Entropy optimized stretching flow based on non-Newtonian radiative nanoliquid under binary chemical reaction. Comput. Methods Programs Biomed. 188, 105274.

Waqas, H., Imran, M., Muhammad, T., Sait, S.M., Ellahi, R., 2021. Numerical investigation on bioconvection flow of Oldroyd-B nanofluid with nonlinear thermal radiation and motile microorganisms over rotating disk. J. Therm. Anal. Calorim. 145 (2), 523–539.

Waqas, M., Khan, W.A., Asghar, Z., 2020. An improved double diffusion analysis of non-Newtonian chemically reactive fluid in frames of variables properties. Int. Commun. Heat Mass Transfer 115, 104524.

Zhang, L., Bhatti, M.M., Ellahi, R., Michaelides, E.E., 2020. Oxytactic microorganisms and thermo-bioconvection nanofluid flow over a porous Riga plate with Darcy–Brinkman–Forchheimer medium. J. Non-Equilib. Thermodyn. 45 (3), 257–268.